Journal of Medicinal Chemistry

Article

pubs.acs.org/jmc

Psoralen Derivatives as Inhibitors of NF-κB/DNA Interaction: Synthesis, Molecular Modeling, 3D-QSAR, and Biological Evaluation

Giovanni Marzaro,[†] Adriano Guiotto,[†] Monica Borgatti,[‡] Alessia Finotti,[‡] Roberto Gambari,[‡] Giulia Breveglieri,[‡] and Adriana Chilin*[,†]

[†]Dipartimento di Scienze del Farmaco, Università degli Studi di Padova, Via Marzolo 5, 35131 Padova, Italy

[‡]Dipartimento di Scienze della Vita e Biotecnologie, Università di Ferrara, Ferrara, Italy

Supporting Information

ABSTRACT: Some new psoralen derivatives were synthesized and evaluated as inhibitors of NF-κB/DNA interaction, with the aim to investigate the structural determinants required to inhibit this interaction. Starting from molecular docking studies, several possible protein binding sites were proposed and several three-dimensional quantitative structure−activity relationship (3D-QSAR) models were built using the docked poses of **29** (the most active psoralen in the series) as templates for alignment of the inhibitors. The selected best model was validated through the prediction of the activity of 17 novel compounds. All the experimental data agreed with the computational experiments, supporting the reliability of the computational approach. The hypothesis about the interaction with NF-κB was also supported by surface plasmon resonance based assays using compound **29**. All the collected data allowed the identification of compound **29** as a potential candidate for the development of pharmaceutical strategies against the inflammatory phenotype of cystic fibrosis.

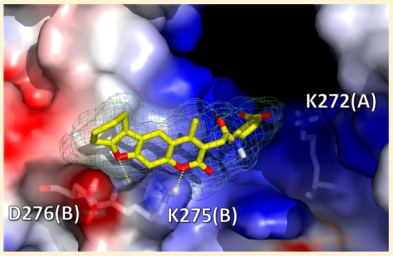

INTRODUCTION

NF-κB is a transcription factor involved in the control of a large number of normal cellular and organism processes, such as immune and inflammatory responses, cellular growth and apoptosis.[1−3] The deregulation of NF-κB is associated with many diseases such as AIDS and other viral infections, arthritis and other inflammatory diseases, cancer, and genetic disorders.[4−7] In this way, targeting NF-κB could be of great interest in order to find new therapeutic agents, mainly anticancer and/or anti-inflammatory compounds. In the case of cystic fibrosis (CF), one of the most important NF-κB regulated targets is the gene coding the proinflammatory cytokine IL-8.[8,9] In fact, IL-8 is the most important inflammatory protein induced by *Pseudomonas aeruginosa* infection.[10,11] With respect to this issue, we have recently characterized the transcriptional control of the human IL-8 gene, demonstrating the role of NF-κB using the transcription factor decoy approach with decoy molecules mimicking NF-κB binding sites.[12] In conclusion, targeting IL-8 gene expression appears to be therapeutically relevant and NF-κB should be considered among the most important molecules to inhibit, in order to achieve anti-inflammatory and IL-8 inhibitory effects on CF cells.

Among NF-κB inhibitors, we found several psoralen derivatives. For instance, 4,6,4′-trimethylangelicin (TMA) was proven to inhibit the recruitment of NF-κB to the IL-8 gene promoter and to exert inhibitory effects on the accumulation of IL-8 mRNA and on the secretion of IL-8 protein.[13] Moreover, other psoralen derivatives able to inhibit NF-κB/DNA interactions and the related IL-8 gene expression were identified.[14−19] On the basis of a combination of different approaches, including virtual screening, molecular docking, electrophoretic mobility shift assay, and expression of NF-κB regulated genes studied by RT-PCR and Bio-plex analyses,[17] we found a good correlation between molecular interaction with the NF-κB factor and inhibition of NF-κB activity studied in cell-free conditions (EMSA) and in cellular systems. In particular, psoralens such as those reported in Figure 1 were considered as interesting leads for the development of pharmaceutical strategies against the inflammatory phenotype of CF, since they exhibited high efficiency in inhibiting NF-κB/DNA interactions and also IL-8 gene expression in TNF-α treated IB3-1 CF cells. Unfortunately, this interesting feature should be considered just as a proof-of-concept based on a limited number of molecules; in agreement, no structure−activity relationship was attempted.

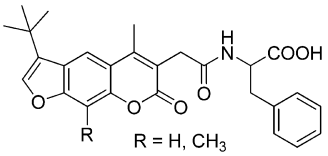

Figure 1. Structure of reference compounds.

With the aim to establish a structure−activity relationship and to define the structural determinants required to inhibit the NF-κB/DNA interaction through NF-κB binding, we synthesized and evaluated several new psoralen derivatives. The

Received: July 5, 2012
Published: February 17, 2013

dx.doi.org/10.1021/jm3009647 | J. Med. Chem. 2013, 56, 1830−1842

binding site of the compounds was proposed by combining molecular docking and 3D-QSAR studies. In fact, although the crystallographic structure of NF-κB was reported,[20] no structure with bound inhibitor was resolved to date. Another major issue with NF-κB is its molecular weight (higher than 37 kDa), which impairs the specific characterization of the whole protein through NMR experiments.[21] Consequently, no information regarding the binding modes of known NF-κB/DNA interaction inhibitors is reported in literature. In the past years, however, the increase in efficiency of computational tools has highlighted the following: (i) molecular docking studies, in particular "blind docking" strategies,[22,23] are useful tools in the identification of putative binding site(s); (ii) robust and effective 3D-QSAR models can also be generated when the tridimensional structure of the binding site is unknown;[24] (iii) validated 3D-QSAR models can be used for the so-called "receptor mapping techniques",[25] which allow the generation of hypothetical model of the binding site (receptor site model).[26] In this respect, a crucial aspect of the 3D-QSAR modeling is the choice of the ligands conformations. Indeed, a major limitation of the "receptor mapping techniques" is that the computed model site is usually derived from the minimized ligands structures that could not correspond to the bioactive conformations.[24] As a consequence, a so computed model site could not perfectly overlap with the real protein binding site.

Thus, in this work we tried to join the useful aspects of molecular docking and 3D-QSAR modeling to derive a binding site for psoralens.

RESULTS AND DISCUSSION

Chemistry. Several structural changes were introduced in the points of diversity of the psoralen structure (Figure 2) to explore the role of specific positions with respect to biological activity, providing a small library of 37 compounds. The two positions of the furan ring were substituted with one or two methyl groups, a *tert*-butyl group, or a further condensed cyclohexane ring, with the aim to investigate the significance of steric hindrance, as well as for the benzene portion, which was unsubstituted or substituted with a methyl function. The chain length in the spacer portion was modulated with one to two methylene spacers. The amide substituent on the side chain was modified, changing the nature and the position of the carboxylic group and also replacing it with a chlorine atom. Thus, the newly synthesized compounds, as reported in Table 1, were grouped in seven series according to furan ring substituents and to the absence or presence of the methyl group on the central benzene ring.

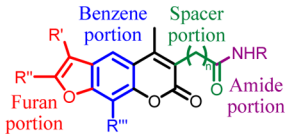

Figure 2. Points of diversity in the psoralen structure.

All the compounds were prepared with the same synthetic strategy that consisted of (i) condensation of the furan ring on the desired alkyl benzopyranylacetate or propionate, (ii) hydrolysis of the ester function, and (iii) final condensation with the opportune amine. In detail, starting (7-oxo-7*H*-furo[3,2-*g*][1]benzopyran-6-yl)acetic or propionic acids were synthesized according to previously reported methods,[27,28] slightly modified to take advantage of MAOS (microwave assisted organic synthesis), as described for compound **2**.[19] Acid derivatives were activated as acyl chlorides and then reacted with the opportune amines or amino acids to give the desired amides, paying attention to reaction temperature to avoid decarboxylation of psoralen acids (Scheme 1).

Screening of Inhibitors of NF-κB/DNA Interaction by EMSA Assays. In order to obtain a first indication on biological activity, electrophoretic mobility shift assays (EMSA) were performed using purified p50 NF-κB protein. This approach represents a standard technology very useful in determining the potency of inhibitors of NF-κB/DNA interactions.[10,15,17] Figure 3 reports a representative EMSA study where compounds were first incubated with NF-κB protein and then the ^{32}P-labeled target NF-κB oligonucleotide was added.

This analysis was performed for all 37 synthesized compounds and used for comparison with chrome azurol (CAS), aurin (AU), pyrocatechol violet (PV), and pyrogallol red (PR), considered as reference compounds. These compounds were reported to bind to the NF-κB DNA-binding domains, leading to inhibition of NF-κB/DNA interactions.[29]

The EC_{50} values, reported in Table 2, showed that the most efficient inhibitors of NF-κB/DNA binding were compounds **4**, **29**, and **32**. Their activity is higher than that found for other known NF-κB inhibitors, such as CAS, AU, PV, and PR, exhibiting inhibition of NF-κB/DNA interactions at EC_{50} ranging between 0.03 and 0.1 mM, as detailed in Table 2.[29]

Since it is well-known that psoralens intercalate into DNA,[30] linear dichroism experiments were performed to determine the intercalative properties of the new derivatives. However, no differences in the dichroic spectra were found between free DNA and DNA incubated with our compounds (see Figure S1 in Supporting Information), thus suggesting that the nucleic acid was not the major target of our psoralen derivatives.

Computational Studies. Since the preliminary biological experiments suggested NF-κB function as the molecular target, docking studies were combined with 3D-QSAR modeling to make a reliable hypothesis on the possible binding mode of the psoralen derivatives to NF-kB protein, following the strategy depicted in Figure 4.

The idea to merge molecular docking with 3D-QSAR modeling to hypothesize a binding site for psoralens arose from the attempt to join the different aspects of the two computational techniques previously mentioned, i.e., (i) to identify putative binding sites through docking studies, (ii) to develop 3D-QSAR models also in the absence of information regarding the binding site, (iii) to extract information on the electrostatic and steric features of the binding site starting from 3D-QSAR models.

Moreover, in the 3D-QSAR modeling, if the compounds alignment is made starting from the crystal (or the docked) pose of a template ligand, the molecular fields can be visualized in context with the protein target, thereby verifying the coherence between the computed model and the protein structure.[31]

Thus, if a good coherence between the steric and the electronic fields of a robust 3D-QSAR model and an NF-κB region were obtained, we could find a plausible binding site for our psoralens. However, instead of generating a receptor site model (which requires other computational studies in addition to 3D-QSAR modeling) and to "move" it on the protein

dx.doi.org/10.1021/jm3009647 | J. Med. Chem. 2013, 56, 1830−1842

Table 1. Synthesized Compounds

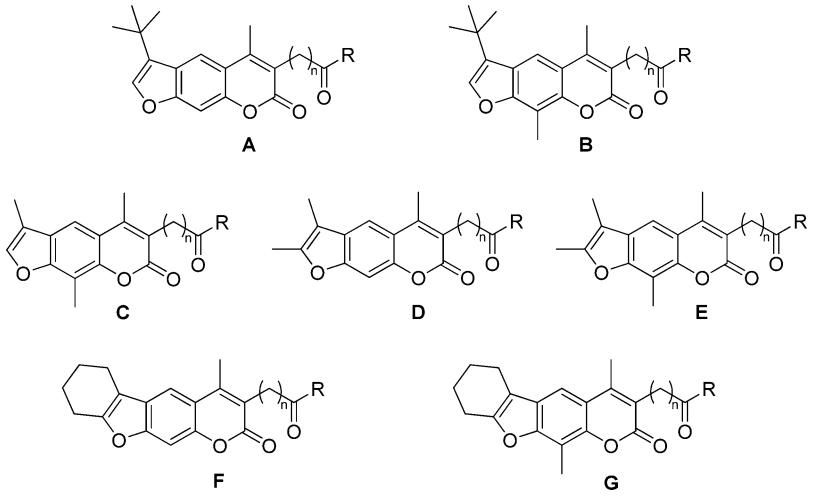

compd	series	n	R	compd	series	n	R
1	A	1		**20**	C	1	
2	A	1	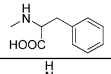	**21**	D	1	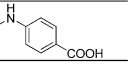
3	A	1	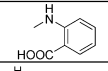	**22**	E	1	
4	A	1	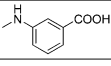	**23**	E	1	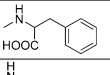
5	A	1	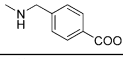	**24**	E	1	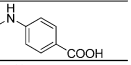
6	A	1	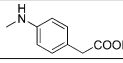	**25**	E	2	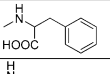
7	A	2	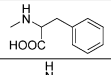	**26**	E	2	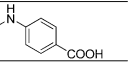
8	A	2	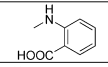	**27**	F	1	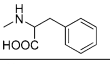
9	A	2	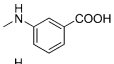	**28**	F	1	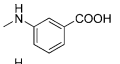
10	A	2	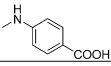	**29**	F	1	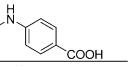
11	A	2	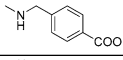	**30**	F	2	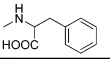
12	A	2	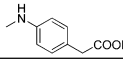	**31**	F	2	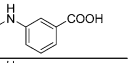
13	B	1		**32**	F	2	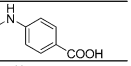
14	B	1	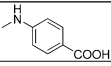	**33**	G	1	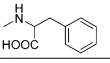
15	B	1		**34**	G	1	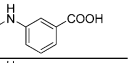
16	B	1	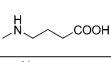	**35**	G	1	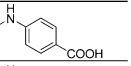
17	B	2	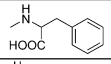	**36**	G	2	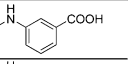
18	B	2	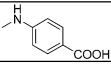	**37**	G	2	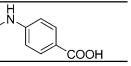
19	B	2					

structure until a full overlap was found, we restricted the protein search space by detecting some putative binding sites through a "blind docking" on compound **29**. In this way, we were able to keep down the computational costs and to propose different reference poses that were in turn used for the psoralens tridimensional alignment.

Docking Studies. The crystal structure of the NF-κB p50–p50 homodimer in complex with DNA (PDB code 1NFK) was

dx.doi.org/10.1021/jm3009647 | *J. Med. Chem.* 2013, 56, 1830–1842

Scheme 1[a]

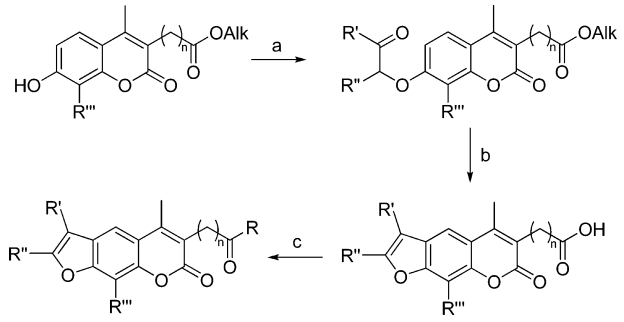

[a]Reagents and conditions: (a) 1-chloropinacolone or chloroacetone or 3-chloro-2-butanone or 2-chlorocyclohexanone, TEA/H_2O, microwave, 130 °C, 20 min;[19] (b) 1 M NaOH, propan-2-ol, microwave, 120 °C, 5 min;[19] (c) (i) $SOCl_2$, rt, 3 h; (ii) amine, THF, TEA/H_2O, rt. See Table 1 for R specification.

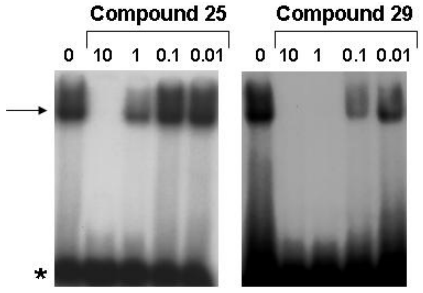

Figure 3. Representative EMSA assays for compounds **25** and **29** with different ability to inhibit NF-κB p50/DNA interaction. 10 ng of human NF-κB p50 protein and different concentrations of compounds were preincubated for 20 min at room temperature. Then 0.25 ng of ^{32}P-labeled DNA/DNA target molecules was added to the samples for a further 20 min at room temperature. Protein/DNA complexes were separated by polyacrylamide gel electrophoresis, and autoradiography was performed. The arrow indicates protein/DNA complexes. The asterisk (*) indicates the free ^{32}P-labeled NF-κB oligonucleotides.

Table 2. EC_{50} Values (mM) To Obtain 50% Inhibition of NF-κB/DNA Interaction

compd	EC_{50}	compd	EC_{50}	compd	EC_{50}
1	0.80	**15**	5.00	**29**	0.01
2	0.60	**16**	0.60	**30**	0.10
3	0.08	**17**	0.06	**31**	0.10
4	0.01	**18**	0.04	**32**	0.01
5	0.60	**19**	4.00	**33**	1.00
6	0.53	**20**	0.80	**34**	0.07
7	0.10	**21**	0.04	**35**	0.10
8	0.06	**22**	6.00	**36**	0.10
9	0.06	**23**	0.60	**37**	0.06
10	0.06	**24**	0.10	PV	0.05
11	0.67	**25**	1.00	AU	0.05
12	0.08	**26**	0.06	PR	0.03
13	0.80	**27**	0.08	CAS	0.10
14	0.06	**28**	0.10		

chosen for the docking studies, employing the AutoDock 4.2 software (see the Experimental Section for a detailed description of the docking experiments). AutoDock consists of two engines, AutoGrid that computes several atom-specific affinity maps along with one electrostatic map and one desolvation map inside the binding site (collected into the

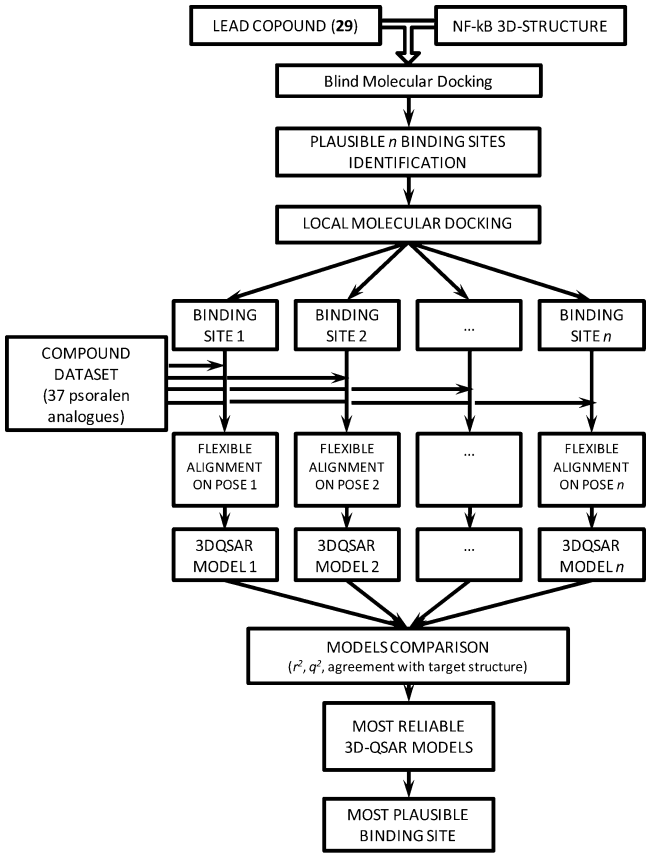

Figure 4. Computational strategy used for the identification of psoralen binding site.

docking box) and AutoDock that performs the conformational analysis and the scoring of the ligand based on the precomputed maps. Initially the docking box was allowed to contain the whole DNA-binding region of the enzyme, thus performing the "blind docking".[22,23] As previously mentioned and in accordance with the EMSA data, at this stage, compound **29** was chosen as "probe", allowing the identification of four putative binding sites. During the "blind docking" procedure, the amide bond of the ligand was left free to rotate. In fact, quantum mechanics (QM) calculations showed that the energy difference between the trans and the cis amide conformations was quite low (2.0 kcal/mol), with the trans conformation characterizing the global minimum. The QM results were also supported by NOESY experiments that showed, among the others, a spatial correlation between the methylene spacer and the amide aromatic ring (possible only in the case of the cis amide conformation; see Figure S2 in Supporting Information). The NOESY spectrum was recorded in DMSO-d_6 instead of D_2O or D_2O/NaOD, although the solvent could affect the conformational equilibrium. In fact, in the presence of a large amount of water, the methylene signal and the water peak fell together, thus impairing the determination of the spatial correlation. However, the QM and the NMR data suggested that we cannot discard the existence of the cis-conformation a priori. Since the blind docking procedure yielded some poses with the amide dihedral quite far from planarity, the docking studies were then performed again to obtain more exhaustive poses. One docking box of appropriate dimensions was centered on each previously determined site. At this stage, the amide rotation was not allowed: the appropriate amide

dx.doi.org/10.1021/jm3009647 | J. Med. Chem. 2013, 56, 1830−1842

conformations were chosen in accordance with the dihedral values obtained in the blind docking (see Table 3). The results of the docking studies are summarized in Figure 5.

Table 3. Conformations of Compound 29 Used in the Docking Refinement Procedure

site	H−N−O−C dihedral (blind docking)[a]	H−N−O−C dihedral (docking refinement)[b]	energy penalty (kcal/mol)[c]
1	30° (cis-like)	0° (cis)	29.7
2	61° (cis-like)	0° (cis)	5.2
3	43° (cis-like)	0° (cis)	21.3
4	180° (trans)	180° (trans)	1.1

[a]Dihedral values measured in the poses obtained in the blind docking studies. [b]Dihedral values forced in the docking refinement procedure (cis conformation was chosen when the dihedral of the blind docking obtained pose was closer to 0° than to 180°; trans conformation was chosen when the dihedral was closer to 180° than to 0°). [c]QM-based energy difference between the docked pose (obtained after the docking refinement protocol) and the global minimum energy (obtained through QM-based structure minimization). All the QM calculations were performed "in water".

In all the cases, the carboxylic function of the compound was found to establish H-bonds with positive charged amino acid residues (Lys144(A) and Lys145(A) in site 1, Arg51(A) in site 2, Lys144(A) in site 3, Lys272(A) and Lys275(B) in site 4), abundant in the DNA-binding region of NF-κB. Moreover, the oxygen atom of the furan ring was also found to interact with amide protons of the backbone. The computed binding scores (ADT scores) were, in all the cases, almost equal, ranging from −6.36 to −6.42, while the QM-based energy differences between the docked poses and the minimized conformation indicated that poses 1 and 3 were less reliable than poses 2 and 4 (see Table 3).

3D-QSAR Modeling. As previously mentioned, the selection of the most probable binding site was then carried out by means of 3D-QSAR studies, through the computation of one model for each of the four putative binding sites. Thus, no binding site was discarded a priori on the basis of the energy penalties derived from the QM calculations. The reliabilities of the sites were assessed on the basis of the statistical parameters of the 3D-QSAR models (r^2, q^2_{lmo}, SDEC, and SDEP) and of the coherence between each model features and the related binding site characteristics. Briefly, all the synthesized compounds were superimposed onto each of the four docked poses of compound **29**, employing the Discovery Studio 3.1 suite.[32] The structures of all the derivatives (except for compound **29**) were considered flexible, and the better superimpositions were, in all the cases, obtained through the "field fit" methodology with 80% steric and 20% electrostatic contributions. As the docking studies had highlighted the importance of the interaction of the carboxylate anion with positively charged residues, the protonation state of the compounds was also considered. Before the superimposition process, all the molecular structures were hydrogenated at pH 7.4 and all the carboxylic functions were negatively charged. The 3D-QSAR models were then built with the Open3-DQSAR[33] software as described in the Experimental Section. The characteristics of the models are summarized in Table 4.

The model built on binding site 1 showed the lowest correlation (r^2 = 0.58), whereas the model built on binding site 3 showed good correlation in training but poor correlation in internal validation (q^2 = 0.25). On the basis of these results, the

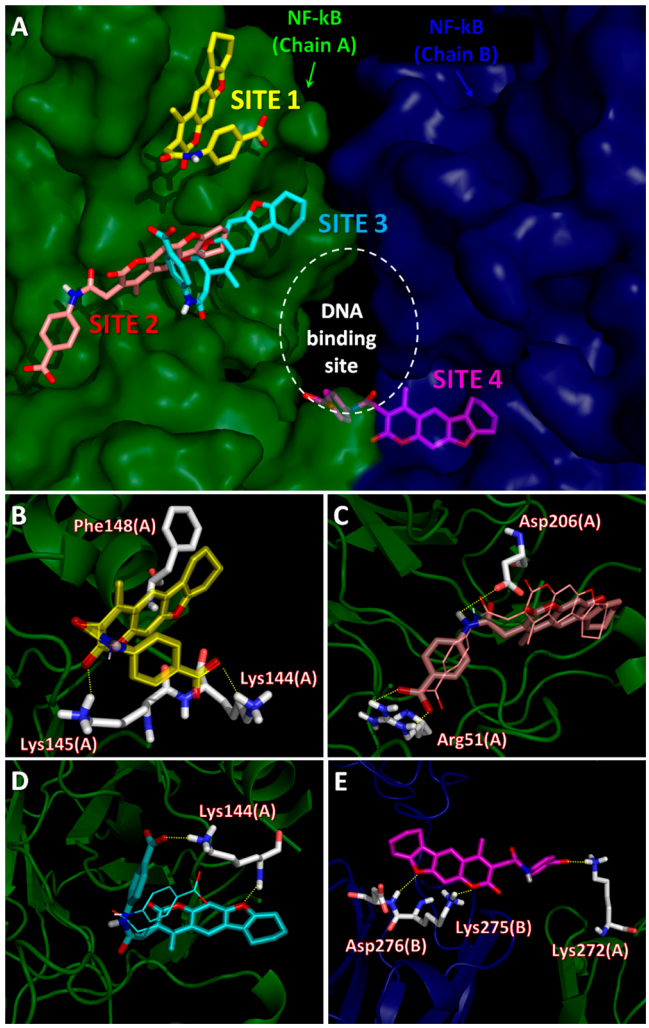

Figure 5. Putative binding sites for psoralen derivatives. (A) Depiction of the four binding sites with respect to the DNA-binding region (white dotted circle) of NF-κB. (B−E) Interactions predicted for compound **29** with protein residues at each site. The hydrogen bonds are highlighted as yellow dotted lines. The poses obtained in the "blind docking" are depicted as lines, while the refined poses are depicted as sticks.

two binding sites were discharged. As reported in Table 4, the number of active variables used for the PC analysis on sites 1 and 3 was considerably higher than the number for sites 2 and 4, reflecting not optimal molecular superimpositions. Indeed, the models 1 and 3 were built on the poses that also showed the highest energy penalties in QM calculations (Table 3). Finally, the number of PCs used was higher than for the models built on sites 2 and 4. Indeed, it is well-known that using a large number of independent variables leads to models with good correlations in training but poor performances in cross-validation or in prediction. Also, binding site 2 was not further considered: although the QSAR model built on this site showed good performances in both training and validation, the molecular fields did not agree with the protein structure. For example, a sterically favorable area clashed against Val209, while a sterically unfavorable area was placed in a protein cavity. On the contrary, the model built on binding site 4, besides showing the best performances, fully agreed with the protein structure (vide post), thus indicating that this could reasonably be the binding site for psoralen derivatives. All the calculated EC_{50}

dx.doi.org/10.1021/jm3009647 | J. Med. Chem. 2013, 56, 1830−1842

Table 4. Statistics of 3D-QSAR Models

binding site	protein residues[a]	r^2	SDEC[b]	q^2_{lmo}	SDEP[c]	active variables[d]	PC[e]
1	Lys144(A) Lys145(A) Phe148(A)	0.579	0.447	0.152	1.050	4234	5
2	Arg51(A)	0.842	0.222	0.654	0.411	1584	3
3	Lys144(A)	0.819	0.273	0.252	0.599	3998	4
4	Lys272(A) Lys275(B) Asp276(B)	0.947	0.163	0.731	0.374	1122	3

[a]Amino acid residues of NF-κB involved in interactions with **29**. [b]Standard deviation error of calculations. [c]Standard deviation error of predictions. [d]Number of independent variables (i.e., sum of the grid points for the steric and for the electrostatic fields retained after the variables reduction procedures described in the Experimental Section) used for the PC analysis. [e]Number of principal components (independent variables) in the model. The number of PCs reported allowed the highest value of q^2.

values, the standard errors, and the leverage values are reported in Table S1 in Supporting Information.

Binding Mode and SAR Analysis. The pseudo coefficients for the steric and the electrostatic fields of the selected model were extracted and visualized to evaluate the agreement of the model with the receptor structure (see an example in Figure 6, and see also Figure S3 in Supporting Information).

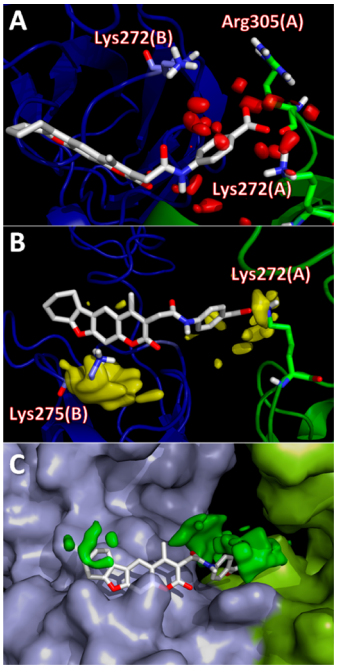

Figure 6. Pseudo coefficients of the selected 3D-QSAR model in context with compound **29** (atom-colored sticks) and the target (cyan and green ribbon backbone in parts A and B; gray and lemon surfaces in part C). Red surfaces indicate negatively charged atoms favorable volumes (level = −0.0008). Yellow surfaces indicate sterically unfavorable volumes (level = −0.0006). Green surfaces indicate sterically favorable volumes (level = +0.0006).

The negatively charged atoms favorable volumes (red surfaces in Figure 6A) were surrounded by positively charged residues (Lys272A, Arg305A, and Lys272B). This finding highlighted the importance of an anionic function in the tested molecules and justified the low activity of compounds not bearing a carboxylic function (**15**, **19**, **20**) or of compounds with a carboxylic function not properly accommodated (e.g., **1**, **13**, **22**; see Figure S4 in Supporting Information). The length of the spacer portion (one or two methylene units) was not fundamental (compare, for example, **29** with **32**), since the terminal carboxylic functions were always located in the same manner (see Figure S5 in Supporting Information). However, in almost all the cases, when an additional methylene function was added to the amide portion (e.g., **5**, **6**, **11**), the activity remarkably decreased (see Figure S6 in Supporting Information). The steric unfavorable areas clashed against Lys272A and Lys275B (yellow surfaces in Figure 6B), whereas the steric favorable areas were well accommodated in the protein cavities (green surfaces in Figure 6C), justifying the slightly lower activities of less hindered compounds (compare, for example, **21** with **29**). On these bases, the selected model also explained why in almost all the cases the presence of a methyl group in the central benzene ring negatively affected the activities (see, for example, **21** in comparison with **24** or **29** in comparison with **35**). We thus supposed that the compounds belonging to classes B, C, E, and G could be accommodated in the binding site only by inducing a change in the position of Lys275(B). To confirm this hypothesis, compound **35** was docked in binding site 4 allowing the Lys275(B) side chain flexibility. Satisfactorily, the obtained pose (Figure 7) fully agreed with that

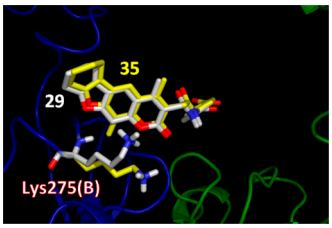

Figure 7. Comparison of the binding modes predicted for compound **29** (white sticks) and compound **35** (yellow sticks). NF-κB is depicted as green and blue colored backbone. The Lys275 residue is depicted in sticks colored accordingly to the related ligand. Note that in the case of compound **35**, the movement of the Lys275 side chain (induced by the presence of the methyl group in the ligand) causes a loss of the hydrogen bond with the pyran ring.

observed for compound **29**. However, the loss of the hydrogen bond between Lys275(B) and the oxygen atom of the pyran ring (due to the induced movement of the amino acid side chain) probably caused the reduction in the binding efficiency ($ADT\text{-}Score_{compd29} = -6.42$; $ADT\text{-}Score_{compd35} = -5.68$).

Validation of the 3D-QSAR Model. In all the previously discarded models, the compounds were characterized by the cis

dx.doi.org/10.1021/jm3009647 | J. Med. Chem. 2013, 56, 1830−1842

Table 5. Compounds in the Test Set and Measured EC_{50} (mM)

compd	series	n	R	EC_{50}	compd	series	n	R	EC_{50}
38	D	1	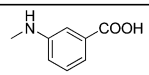	0.70	**47**	G	1	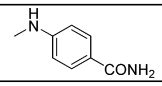	0.70
39	D	2	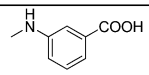	0.60	**48**	G	2	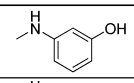	0.70
40	E	1	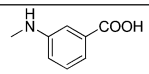	0.60	**49**	G	2	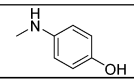	3.00
41	E	2	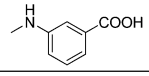	0.08	**50**	G	2	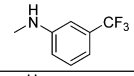	>10
42	G	1	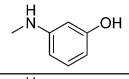	3.00	**51**	G	2	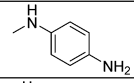	3.00
43	G	1	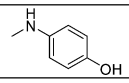	0.70	**52**	G	2	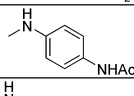	1.00
44	G	1	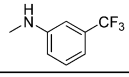	3.00	**53**	G	2	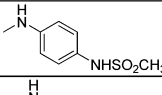	1.00
45	G	1	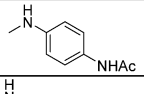	3.00	**54**	G	2	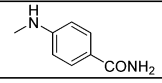	0.70
46	G	1	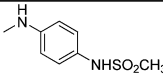	0.70					

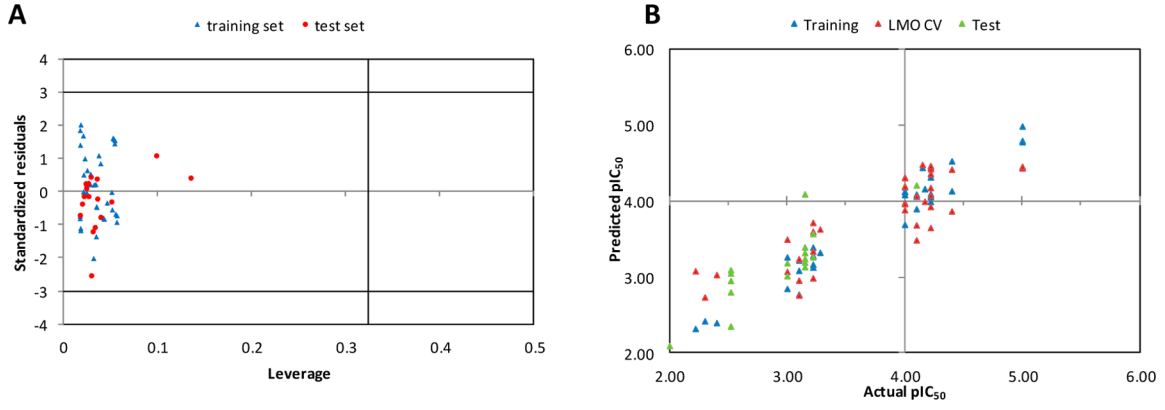

Figure 8. Selected 3D-QSAR model. (A) Williams' plot indicating the applicability domain of the model. As all the compounds fall within ±3 standard deviation units (horizontal lines) and have a leverage lower than the critical value (0.324 for the present model, vertical line), no outliers were present. (B) Actual versus predicted pEC_{50} for psoralen derivatives in training (blue triangles), cross-validated (red triangles), and test (green triangles) sets.

amide conformations. In order to exclude that the selected model outperformed the others only because of trans amide conformations, an additional model was also built using the fully minimized conformation of compound **29** as a template for the molecular alignment. However, in this case also, lower statistical parameters were found (r^2 = 0.74; q^2 = 0.42), suggesting that the active conformations could be different from the lowest energy ones, as observed in many other cases.[34] Also in this case, it cannot be stated that this is a confirmation that site 4 is the real binding site for psoralens, but the computational approach allowed us to propose at least reasonable bioactive conformations.

The selected model was then used to predict the EC_{50} values of a number of properly synthesized psoralen derivatives (Table 5). Following a previously reported approach,[31] in order to test the model, compounds structurally very close to those used in the training set were included in the test set (**38**–**41**) as well as molecules whose properties vary significantly (**42**–**54**), mainly in terms of pK_a properties and H-bond donor/acceptor characteristics.

All the 17 molecules were synthesized with the same synthetic strategy depicted in Scheme 1 and were evaluated by means of EMSA experiments. The QSAR model was found to predict in a very satisfactory manner the activities of the novel compounds ($r^2_{prediction}$ = 0.73, SDEP = 0.26; see Table S1 in Supporting Information for all the calculated EC_{50} values, the standard errors, and the leverage values). Interestingly, when the activities were predicted with the discarded 3D-QSAR models, very low correlations were found, with r^2 of prediction ranging from 0.21 to 0.32.

None of the newly synthesized derivatives were more active than parent compound **29**. These data confirmed the importance of a bulky substituted furan (compare compounds **38**–**41** with **29**) and of a terminal residue (i.e., the carboxylate

dx.doi.org/10.1021/jm3009647 | J. Med. Chem. 2013, 56, 1830–1842

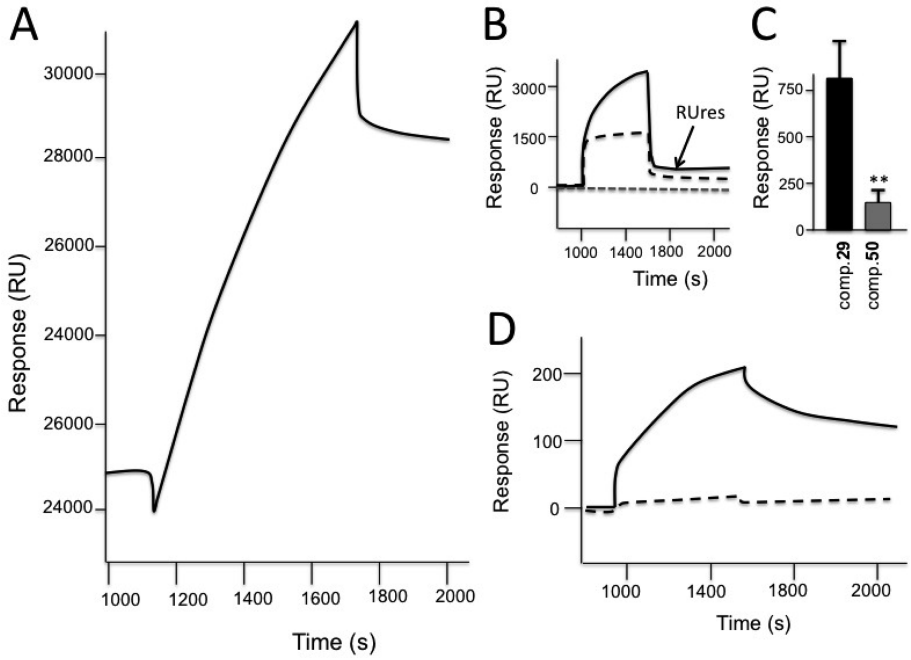

Figure 9. BIA analysis of the binding of compound **29** to NF-κB. (A) Immobilization of NF-κB p50 on the sensor chip CM5 (research grade) by the amine coupling procedure, as described in the Experimental Section. (B) Representative sensorgrams obtained after injection of compound **29** and compound **50**. Stable interactions are represented by RUres (residual RUs). (C) Summary of the bindings of **29** and **50** obtained in three independent experiments. The presented results are the RU ± SD bound to the NF-κB sensor chip. (D) Bindings of the double stranded oligonucleotide 5′-CGCTGGGGACTTTCCACGG-3′ (sense strand) to the NF-κB sensor chip in the absence (solid line) or in the presence (dotted line) of preloaded compound **29**.

anion) able to form strong interactions with the positively charged amino acids present in the DNA binding region of the transcription factor.

Finally, the domain of applicability was also determined (Figure 8).[35] As no outliers were identified, all 54 compounds fit into the 3D-QSAR model.

Surface Plasmon Resonance (SPR) Based Biospecific Interaction Analysis (BIA) of Interactions between Compound 29 and NF-κB. Since the docking experiments suggested a direct binding of compound **29** to NF-κB, this possibility was also investigated through biospecific interaction analysis using the SPR-based biosensor BIAcore X-100 (Biacore, GE Healthcare). We first immobilized NF-κB p50 on a CM5 sensor chip using the amine coupling technology (see the representative binding sensorgram shown in Figure 9A). Then we injected **29** (which was proposed to display highly efficient binding to NF-κB) and **50** (which was proposed to display low efficient binding to NF-κB). The results obtained (depicted in Figure 9B and Figure 9C) suggested that compound **29** was able to bind to NF-κB immobilized on the sensor chip with higher efficiency than compound **50**. In three independent interactions experiments 765.5 ± 150 RU representing stable complexes between compound **29** and 7139.5 ± 250 RU of immobilized NF-κB were found (Figure 9C). As a matter of fact, by this approach the binding site was not precisely definable, as well as the stoichiometry of the binding. However, taken together, the obtained results are compatible with binding of compound **29** to the NF-κB factor. In addition, it is important to emphasize that the same experiment done with compound **50** showed a significant lower binding activity (Figure 9C), in agreement with the computational studies. The SPR-based BIA analysis not only supported the conclusions driven by the docking approach but was fully consistent with the EMSA experiments. In fact, when a double stranded oligonucleotide on the NF-κB sensor chip preloaded with compound **29** was injected, a full inhibition of DNA/NF-κB interaction was observed (Figure 9C). While the possibility that interaction of compound **29** with NF-kB might lead to additional effects altering NF-kB/DNA interactions (including, but not limited to, unfolding, even partial, of NF-kB) cannot be ruled out, the BIA data supported the EMSA results and suggested that compound **29** deserves further studies to determine its possible inhibitory activity on NF-kB dependent genes, including IL-8.

Effects of Compound 29 on the Expression of IL-8 Genes in TNF-α Treated IB3-1 Cells. Since the EMSA experiments agreed in indicating psoralen **29** as the most interesting NF-κB inhibitor, the study on the effect on cystic fibrosis cell line was performed with this compound.

In order to determine the effects on IL-8 mRNA accumulation, the expression of IL-8 gene was studied by RT-PCR analysis of RNA extracted from TNF-α treated CF IB3-1 cells cultured in the presence of increasing concentrations of compound **29** for 24 h. As already pointed out, the accumulation of IL-8 mRNA was chosen to be analyzed because IL-8 is one of the most expressed interleukins involved in inflammatory processes and is strongly induced by TNF-α treatment.[36]

Figure 10A shows the results obtained by quantitative RT-PCR concerning the effects of compound **29** on TNF-α induced IL-8 mRNA accumulation in cell. A clear induction of IL-8 transcripts following TNF-α treatment was evident (CTRL+). Significant inhibitory effects on IL-8 mRNA accumulation were detected following exposure of TNF-α induced IB3-1 cells to compound **29**.

dx.doi.org/10.1021/jm3009647 | J. Med. Chem. 2013, 56, 1830−1842

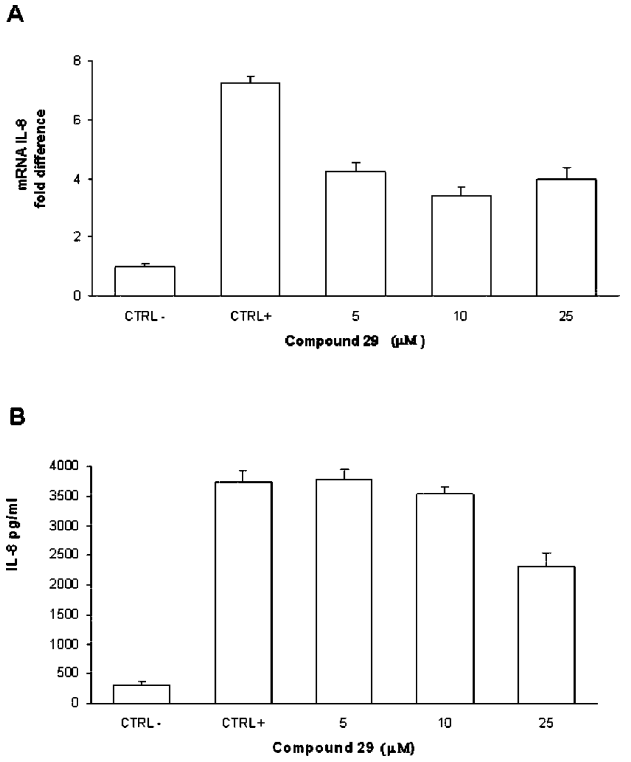

Figure 10. Effects of compound **29** on TNF-α induced IL-8 gene expression in IB3-1 cells: (A) quantitative RT-PCR analysis of IL-8 mRNA fold difference relative to untreated cells (CTRL −); (B) Bio-plex analysis of IL-8 protein present in supernatants; (CTRL −) untreated IB3-1 cells; (CTRL +) TNF-α treated IB3-1 cells. For each experiment duplicate RT-PCR determinations were performed. Results represent the average ± SD of three independent experiments.

These results were also confirmed using Bio-plex technology to analyze the release of IL-8 protein (pg/mL) in supernatants collected from the same IB3-1 cells induced with TNF-α and treated with compound **29**. The results, shown in Figure 10B, confirmed the inhibitory activity of compound **29** on expression of IL-8 protein in IB3-1 cells at 25 μM. These data suggest that compound **29** might specifically inhibit the expression of the IL-8 proinflammatory gene.

To ensure that the reduction in IL-8 expression did not arise from the impairment of cell viability, the IC_{50} of compound **29** was determined and cell viability evaluated by trypan blue exclusion test. The measured IC_{50} was 355 ± 9.2 μM; thus, it can be excluded that the measured biological properties of the compound could be due to cytotoxic effects.

CONCLUSION

NF-κB is a very important transcription factor involved in several human pathologies, including osteoporosis,[37] rheumatoid arthritis,[38] and cancer.[39,40] In addition, NF-κB is one of the master transcription factors responsible for inflammation in CF cells infected with *Pseudomonas aeruginosa*.[11] Accordingly, compounds that bind to NF-κB, thus interfering with the NF-κB/DNA interaction and inhibiting IL-8 expression in CF cells, are of great importance.[10]

Starting from the structure of the previously reported psoralen derivatives depicted in Figure 1, several novel analogues have been synthesized. Four points of structural diversity have been considered: (i) the furan substituents; (ii) the presence/absence of a methyl in the central benzene ring; (iii) the length of the spacer between the psoralen nucleus and the amide function; (iv) the nature of the amide moiety. The evaluation of the inhibition of the NF-κB/DNA interaction through EMSA analysis allowed the identification of **29** as the most promising compound in the series. By use of **29** as reference compound in molecular docking studies, four hypothetical binding sites have been proposed. Then the selection of the most plausible binding site was obtained by comparison of several 3D-QSAR models. The final selected model was validated through the prediction of the activities of the other 17 psoralen derivatives, whose structural features were quite different from those of the molecules in the training set. The computational methodologies allowed also the definition of a structure−activity relationship. In particular, with respect to the four points of diversity, (i) the presence of a steric hindrance on the furan ring positively modulated the ability to inhibit the protein−DNA interaction, (ii) the presence of a methyl group in the central benzene ring caused a reduction in activity, (iii) the length of the spacer portion (one or two methylene units) did not significantly influenced the activities, and (iv) the amide moiety required a terminal carboxylic function that probably interacted with positively charged amino acids (as Lys and Arg).

To the best of our knowledge, this work constitutes the first example of the combination of molecular docking and 3D-QSAR modeling to propose a hypothetical binding mode. Although it was not possible to demonstrate the accuracy of the proposed binding site with structural evidence, all the experimental data fully agreed with the computational experiments, thus supporting, at least in part, the potential of the proposed computational strategy. The selected model will be used in the future for the rational design of novel and more potent inhibitors.

The hypothesis of the binding of compound **29** to NF-κB was further supported by the results obtained through biospecific interaction analysis. The results were compatible with the binding of compound **29** to NF-κB, leading to stable formation of a complex that prevented the binding of NF-κB to oligonucleotides, in full agreement with the EMSA experiments. These data suggested that the interaction of compound **29** with NF-κB played a key role in the inhibition of NF-κB/DNA interactions. Furthermore, the inhibition of the NF-κB/DNA interaction by preloaded compound **29** on immobilized NF-κB suggested a binding to the DNA-binding site of NF-κB, in agreement with molecular docking and 3D-QSAR studies.

Clearly, further efforts will be necessary to determine whether compound **29** has a unique binding site and, more importantly, the accuracy of the proposed binding site. In this respect BIA experiments might be repeated using mutant NF-kB proteins and/or recombinant NF-kB contructs mimicking specific domains of NF-kB. In addition to the SPR-based BIA approach, other technologies might be highly recommended, including NMR of specific $^{13}C-^{15}N$ labeled domains of the protein.

Despite the fact that the data do not fully explain the inhibition of NF-kB/DNA interaction by compound **29** and do not allow exclusion of interactions of compound **29** with other proteins/molecules present in tissue culture conditions or within the cellular system employed, the collected biological data suggest possible biomedical applications of compound **29**. In this respect, it is relevant that NF-κB inhibitors, such as parthenolide[41] and azithromycin,[42] are employed in clinical

trials for CF; thus, compound **29** could also be an interesting candidate for CF treatment.

Taken together, these data indicate that psoralens belonging to this set might find an important place in the set of molecules of interest for the development of pharmaceutical strategies against the inflammatory phenotype of CF.

EXPERIMENTAL SECTION

Chemistry. All commercial chemicals and solvents used were analytical grade and were used without further purification. Analytical thin layer chromatography (TLC) was performed on precoated silica gel plates (Merck 60-F-254, 0.25 mm). Melting points were determined on a Gallenkamp MFB-595-010M melting point apparatus and are uncorrected. The ^{1}H NMR spectra were recorded on a Bruker 300-AMX spectrometer with TMS as an internal standard. Coupling constants are given in Hz, and the relative peaks area were in agreement with all assignments. Elemental analyses were performed on a Perkin-Elmer 2400 analyzer. Mass spectra were obtained using a Applied Biosystem Mariner system 5220 with direct injection of the sample. Starting (3′-*tert*-butyl-5′-methyl-7′-oxo-7*H*-furo[3,2-*g*][1]-benzopyran-6′-yl)acetic and propionic acids (type A), (3′-*tert*-butyl-5′,9′-dimethyl-7′-oxo-7*H*-furo[3,2-*g*][1]benzopyran-6′-yl)acetic and propionic acids (type B), (3′,5′,9′-trimethyl-7′-oxo-7*H*-furo[3,2-*g*][1]-benzopyran-6′-yl)acetic acid (type C), (2′,3′,5′-trimethyl-7′-oxo-7*H*-furo[3,2-*g*][1]benzopyran-6′-yl)acetic acid (type D), (2′,3′,5′,9′-tetramethyl-7′-oxo-7*H*-furo[3,2-*g*][1]benzopyran-6′-yl)acetic and propionic acids (type E), (4′-methyl-2′-oxo-6′,7′,8′,9′-tetrahydrobenzofuro[3,2-*g*]-1-benzopyran-3′-yl)acetic and propionic acids (type F), (4′,11′-dimethyl-2′-oxo-6′,7′,8′,9′-tetrahydrobenzofuro[3,2-*g*]-1-benzopyran-3′-yl)acetic and propionic acids (type G) were prepared according to literature methods,[27,28,43] modified as described for the already reported compound **2**.[19] All the amine reagents (2-aminobenzoic acid, 3-aminobenzoic acid, 4-aminobenzoic acid, 4-aminomethylbenzoic acid, 4-aminophenylacetic acid, DL-phenylalanine, 2-chlorobenzylamine, 4-aminobutyric acid, 3-aminophenol, 4-aminophenol, 3-trifluoromethylaniline, 4-amino-*N*-acetylaniline, 4-amino-*N*-methanesulfonylaniline, 4-aminobenzamide, *p*-phenylendiamine) were used as purchased. Purity for all the tested compounds was determined by elemental analyses and was found to be equal to or more than 95%.

General Procedures for Amides 3−12, 14−21, and 23−54. A solution of the above-mentioned starting acid (1.0 mmol) in thionyl chloride (25 mL) was stirred at room temperature until a clear solution was formed. The solvent was evaporated under a nitrogen stream at room temperature, and the residue was dissolved in dry tetrahydrofuran (10 mL). The solution was added dropwise to a mixture of the amine (2.0 mmol) in triethylamine (0.3 mL, 2.1 mmol) and water (5 mL). After reaction completion, the mixture was diluted with water (40 mL) and acidified with 1 M HCl to pH 3. The resulting precipitate was filtered off and crystallized from propan-2-ol to give **3−12**, **14−21**, **23−54**.

See Supporting Information for the data of all the synthesized compounds.

Computational Methodologies. All the computational studies were carried out on a 4 CPU (Intel Core2 Quad CPU Q9550, 2.83 GHz) ACPI x64 Linux workstation with Ubuntu 12.04 operating system. The NF-κB/DNA complex structure was downloaded from Protein Data Bank (PDB code 1NFK) and modified with Chimera 5.3.1 software.[44] All the QM studies have been performed with Firefly 8.0 software at the B3LYP level with 6-31+G(d,p) basis set. All the input files for Firefly have been prepared with the graphical interface of Avogadro 1.1.0 software. For the molecular docking and the 3D-QSAR studies, the psoralen structures have been prepared with MarvinSketch 5.5 software.[45] The lowest energy conformations and the degree of protonation at pH 7.4 were determined with OpenBabel 2.2.3 software,[46] using the MMFF94s force field. All the docking studies have been performed with AutoDock (AD) 4.2 software with AutoDock Tools 1.5.4 (ADT) graphical interface.[47] For compound **29** and **35**, the Gasteiger charges were computed and the nonpolar hydrogen atoms were merged with ADT, thus preparing the appropriate PDBQT files for the molecular docking studies. The superimpositions of molecules have been done using the Discovery Studio 3.1 suite.[32] All the 3D-QSAR studies have been performed using Open3DQSAR 2.02 software.[33]

Blind Molecular Docking. The structure of NF-κB in complex with the DNA has been imported in Chimera, and the water molecules and the nucleic acid were removed. The so handled protein structure was imported in ADT. The hydrogen atoms were added, and the Gastaiger charges were computed. After the addition of the AutoDock atom types the nonpolar hydrogen atoms were merged and the protein was saved in PDBQT file format required for AutoDock and AutoGrid tools. The entire protein structure has been contained in a box (coordinate of the center: $x = -2.37$, $y = 13.23$, $z = 19.60$) with 0.55 Å grid spacing and 80 × 80 × 80 points in order to allow the computation of the atom-affinity maps through AutoGrid 4.2 application. The molecular docking simulations were then performed with AD, using compound **29** as flexible ligand and with the searching parameters previously reported for the blind docking strategy.[23] The amide bond of compound **29** was left free to rotate. Cluster analysis was performed on docked results, with a root-mean-square tolerance of 2.0 Å. All the poses with binding energy ranging from the minimum ADT-Score to ADT-Score + 1 were then extracted, leading to the identification of four different plausible binding sites for psoralen derivatives.

Binding Poses Refinement. A docking refinement study has been performed at each of the previously determined binding sites. In all the cases, the boxes for AutoGrid were characterized by 0.375 Å spacing and by 54 × 54 × 54 points. The boxes were centered at $x = 12.43$, $y = 2.50$, $z = 21.80$ (site 1); $x = 11.92$, $y = 18.50$, $z = 20.68$ (site 2); $x = 6.27$, $y = 12.09$, $z = 20.78$ (site 3); $x = -11.11$, $y = 18.23$, $z = 15.33$ (site 4). For each site, a total of 10 runs with a maximum of 2 500 000 energy evaluations were carried out, using the Lamarkian genetic algorithm (LGA) searching engine. At each site, the amide bond of compound **29** was constrained to the cis conformation or the trans conformation, depending on the dihedral angle determined in the "blind docking" procedure (see Table 3). Cluster analysis was performed on docked results, with a root-mean-square tolerance of 2.0 Å, finally selecting the lowest energy pose.

Quantum Mechanical Studies. The fully minimized structure of compound **29** (trans amide conformation) has been determined with the Firefly QC package[48] (which is partially based on the GAMESS-US source code),[49] setting the parameters as follows: $basis gbasis = N31 ngasuss = 6 ndfunc = 1; npfunc = 1; dffsp = .true.; $pcm solvnt = water; $contrl scftyp = rohf; runtyp = energy; dfttyp = b3lyp; icharge = −1; mult = 1. The minimized structure of compound **29** with the cis amide conformation has been determined using the same parameters, with the amide dihedral angle constrained at 0°. All the QM-based energies have been computed using the same parameters as above, with the only exception of runtyp, which was set to "energy".

Flexible Target Molecular Docking. The PDBQT file of NF-κB was modified, allowing the Lys275(B) side chain flexibility. The box for AutoGrid was characterized by 0.375 Å spacing and by 54 × 54 × 54 points. The grid was centered at $x = -11.11$, $y = 18.23$, $z = 15.33$. The molecular docking simulation was then performed with AD using compound **35** as flexible ligand and with the searching parameters described in the section "Binding Poses Refinement".

3D-QSAR Modeling. The alignments of the compounds were performed with the Discovery Studio 3.1 suite, using the "field fit" algorithm. This methodology is based on the computation of a steric and an electrostatic field for each molecule. Then the molecules are superimposed in a manner such that the differences among the computed fields are lower than possible. In the present case, the contributions to the alignment were 80% for the steric field and 20% for the electrostatic one. Compound **29** was considered as the rigid template, using the coordinates previously determined through the molecular docking studies (for the models built on the four putative binding sites) or the QM-based fully minimized structure. All the other molecular structures were considered flexible. The torsional increments were set to 10° for all the rotatable bonds except for the amide

dx.doi.org/10.1021/jm3009647 | J. Med. Chem. 2013, 56, 1830−1842

bonds whose torsion values were set to 180° or to 0°, depending on the amide conformations determined in the docking studies. The aligned data sets were used for the computation of five 3D-QSAR models. The steric field (calculated using an sp^3-hybridized carbon atom as probe) and a molecular mechanics based electrostatic field were computed in a grid box that exceeded the largest molecule of 1 Å in all directions. For both fields, a cutoff of 10 kcal/mol was used. The variables with values lower than 0.05 were zeroed, while the variables with standard deviations lower than 0.1 were removed. The active variables retained after these variables reduction procedures were grouped following the smart region definition approach described by Pastor et al.[50] Then the subset of variables that allowed the computation of the model with the higher q^2 value was selected by means of fractional factorial design.[51] In all the cases, the models were cross-validated by means of 20% leave-multiple-out methodology. The q^2 values were used to determine the adequate number of principal components. The full list of commands inputted in Open3DQSAR is reported in Supporting Information. Compounds **1**−**37** were used for the generation and the cross-validation of the 3D-QSAR models. Compounds **38**−**54** were used for the external validation.

Biology. Electrophoretic Mobility Shift Assay (EMSA). EMSA was perfomed as previously described.[52] Briefly, double-stranded synthetic oligodeoxynucleotides mimicking the NF-κB binding (NF-κB, sense: 5′-CGC TGG GGA CTT TCC ACG G-3′) were employed. Oligodeoxynucleotides were labeled with γ^{32}P-ATP using 10 units of T4-polynucleotide-kinase (MBI Fermentas) in 500 mM Tris-HCl, pH 7.6, 100 mM $MgCl_2$, 50 mM DTT, 1 mM spermidine, 1 mM EDTA in the presence of 50 mCi γ^{32}P-ATP in a volume of 20 μL for 45 min at 37 °C. The mixture were brought to 150 mM NaCl, and 150 ng of complementary oligodeoxynucleotide was added. Reaction temperature was increased to 100 °C for 5 min and left diminishing to room temperature overnight. Binding reactions were set up in a total volume of 20 μL containing buffer TF plus 5% glycerol, 1 mM dithiothreitol, 10 ng of human NF-κB p50 protein with or without 10 ng of NF-κB p65 protein (Promega) and different concentrations of compounds. After an incubation of 20 min at room temperature, 0.25 ng of ^{32}P-labeled oligonucleotides was added to the samples for further 20 min at room temperature, and then they were electrophoresed at constant voltage (200 V) under low ionic strength conditions (0.25× TBE buffer of 22 mM Tris borate and 0.4 mM EDTA) on 6% polyacrylamide gels. Gels were dried and subjected to standard autoradiographic procedures.

BIA Technology. Interactions of selected compounds and NF-κB were studied by surface plasmon resonance (SPR) analysis on BIAcore X-100 (Biacore, GE Healthcare).[53,54] The sensor chip CM5 (research grade), with a carboxymethylated dextran matrix, was used. CM5 sensor chips containing NF-κB were obtained by the amine coupling procedure: Briefly, after activation of carboxyl groups on the sensor chip surface by a 70 μL pulse of a solution, 0.2 M 1-ethyl-3-(3-dimethylaminopropyl)carbodiimide (EDC), 0.05 M *N*-hydroxysuccinimide (NHS) (10 μL/min flow rate), 50 μL of NF-κB (12.8 μg/mL) were injected with a flow rate of 5 μL/min. A 70 μL pulse of 1 M ethanolamine (10 μL/min flow rate) was finally performed to deactivate excess reactive groups. Binding to selected compounds (1 mM) or double stranded DNA carrying NF-κB binding sequence (28 μg/mL) was performed in HBS buffer (10 mM Hepes, pH 7.4, 150 mM NaCl, 3.4 mM EDTA, and 0.05% surfactant P2). All procedures were performed at 25 °C and at a 5 μL/min flow rate.

Cell Cultures. IB3-1 cells (LGC Promochem), derived from a CF patient with a ΔF508/W1282X mutant genotype and immortalized with adeno12/SV40,[55] were grown in LHC-8 basal medium (Invitrogen, Carlsbad, CA), supplemented with 5% FBS in the absence of gentamycin, at 37 °C/5% CO_2. For the proliferation assay, IB3-1 cells were seeded at a density of 60 000 cells in 24-well plates in LHC-8 medium in the presence of 5% FBS and drug was added at serial dilutions and incubated for a further 3 days. After this period cells were detached with trypsin/EDTA and resuspended in LHC-8 medium and 5% FBS. The cell number per milliliter was determined by a ZF Coulter counter (Coulter Electronics, Hialeah, FL, U.S.) to obtain IC_{50} concentration and cell viability evaluated by trypan blue exclusion test.

Quantitation of IL-8 Transcripts. Total RNA was isolated (TRIzol Reagent, Sigma-Aldrich, WI, U.S.) and retrotranscribed (Promega Corporation, Madison, WI, U.S.). The resulting cDNA was quantified by relative quantitative RT-PCR. The sequences of the oligonucleotides used for amplification of IL-8 mRNA were 5′-GTG CAG TTTT GCG GAC AAG T-3′ (forward) and 5′-TTA TGA ATT CTC AGC CCT CTT CAA AAA CTT CTC-3′ (reverse). For GAPDH mRNA, they were 5′-AAG GTC GGA GTC AAC GGA TTT -3′ (forward) and 5′-ACTG TGG TCA TGA GTC CTT CCA-3′ (reverse). Each 25 μL of total reaction volume contained 1 μL of cDNA, 10 pmol of primers, 1 × iQ SYBR Green Supermix (Bio-Rad Laboratories, Hercules, CA). RT-PCR reactions were performed for a total of 40 cycles (95 °C for 10 s, 68 °C for 30 s, and 72 °C for 60 s) using an iCycler IQ (Bio-Rad Laboratories, Hercules, CA). The relative proportions of each template amplified were determined based on the threshold cycle (Tc) value for each PCR reaction. The ΔΔCt method was used to compare gene expression data. RT-PCR was usually performed in duplicate using two cDNA preparations for each independent experiment. Changes in mRNA expression level were calculated following normalization with the GAPDH calibrator gene and expressed as fold change over untreated samples. Mean ± SD values were determined for each fold difference for at least three independent experiments.

IL-8 Release. IL-8 in tissue culture supernatants released from the cells under analysis was measured by Bio-Plex cytokine assay (Bio-Rad Laboratories, Hercules, CA)[56] as described by the manufacturer. The premixed multiplex beads of the IL-8 human cytokine were used. An amount of 50 μL of IL-8 standards or samples (supernatants recovered from treated cells) was incubated with 50 μL of anti-IL-8 conjugated beads in 96-well filter plates for 30 min at room temperature with shaking. Plates were then washed by vacuum filtration three times with 100 μL of Bio-Plex wash buffer. An amount of 25 μL of diluted detection antibodies was added, and plates were incubated for 30 min at room temperature with shaking. After three filter washes, 50 μL of streptavidin−phycoerythrin was added, and the plates were incubated for 10 min at room temperature with shaking. Finally, plates were washed by vacuum filtration three times, beads were suspended in Bio-Plex assay buffer, and samples were analyzed on a Bio-Rad 96-well plate reader using the Bio-Plex suspension array system and Bio-Plex Manager software (Bio-Rad Laboratories, Hercules, CA).

■ ASSOCIATED CONTENT

Ⓢ Supporting Information

Results of LD measurements; NOESY spectra of compound **29**; results of the compounds superimposition and pseudo-coefficients for the steric and electrostatic fields of the selected model; superimposition of compounds **29** and **1**, **29** and **32**, **29** and **5**; actual and predicted EC_{50} values, standardized residuals, and leverage values of psoralen derivatives; detailed data of all the synthesized compounds; list of commands used to compute the 3D-QSAR models. This material is available free of charge via the Internet at http://pubs.acs.org.

■ AUTHOR INFORMATION

Corresponding Author

*Phone: 00390498275349. E-mail: adriana.chilin@unipd.it.

Notes

The authors declare no competing financial interest.

■ ACKNOWLEDGMENTS

The project was supported by Telethon (Grant GGP10124), CIB (Consorzio Interuniversitario di Biotecnologie), and FFC (Italian Cystic Fibrosis Research Foundation, Contract FFC#2/2010). The BIAcore X-100 was obtained with "Fondo Grandi

Attrezzature of Ferrara University". M.B. is supported by Chiesi Foundation-2011 and FFC (Italian Cystic Fibrosis Research Foundation, Grant FFC#1/2012).

■ ABBREVIATIONS USED

AD, AutoDock; ADT, AutoDockTools; CF, cystic fibrosis; BIA, biospecific interaction analysis; DMSO, dimethylsulfoxide; DTT, dithiothreitol; EDTA, ethylediaminetetraacetic acid; EMSA, electrophoretic mobility shift assay; ESI-TOF, electrospray ionization time of flight; FBS, fetal bovine serum; HRMS, high resolution mass spectrometry; IL-8, interleukine 8; MAOS, microwave assisted organic synthesis; NMR, nuclear magnetic resonace; NOESY, nuclear Overhauser effect spectroscopy; PDB, Protein Data Bank; QSAR, quantitative structure−activity relationship; RT-PCR, real time polymerase chain reaction; SDEC, standard deviation error of calculations; SDEP, standard deviation error of predictions; SPR, surface plasmon resonance; TBE, Tris/borate/ethylediaminetetraacetic acid; TEA, triethylamine; TLC, thin layer chromatography; TMA, 4,6,4′-trimethylangelicin; TNF, tumor necrosis factor

■ REFERENCES

(1) Hayden, M. S.; Ghosh, S. NF-kappaB, the first quarter-century: remarkable progress and outstanding questions. *Genes Dev.* **2012**, *26*, 203−234.

(2) Brown, K. D.; Claudio, E.; Siebenlist, U. The roles of the classical and alternative nuclear factor-kappaB pathways: potential implications for autoimmunity and rheumatoid arthritis. *Arthritis Res. Ther.* **2008**, *10*, 212.

(3) Siebenlist, U.; Franzoso, G.; Brown, K. Structure, regulation and function of NF-kappa B. *Annu. Rev. Cell Biol.* **1994**, *10*, 405−455.

(4) Perkins, N. D. The diverse and complex roles of NF-kappaB subunits in cancer. *Nat. Rev. Cancer* **2012**, *12*, 121−132.

(5) Victoriano, A. F.; Okamoto, T. Transcriptional control of HIV replication by multiple modulators and their implication for a novel antiviral therapy. *AIDS Res. Hum. Retroviruses* **2012**, *28*, 125−138.

(6) Batra, S.; Balamayooran, G.; Sahoo, M. K. Nuclear factor-kappaB: a key regulator in health and disease of lungs. *Arch. Immunol. Ther. Exp.* **2011**, *59*, 335−351.

(7) Ben-Neriah, Y.; Karin, M. Inflammation meets cancer, with NF-kappaB as the matchmaker. *Nat. Immunol.* **2011**, *12*, 715−723.

(8) Black, H. R.; Yankaskas, J. R.; Johnson, L. G.; Noah, T. L. Interleukin-8 production by cystic fibrosis nasal epithelial cells after tumor necrosis factor-alpha and respiratory syncytial virus stimulation. *Am. J. Respir. Cell Mol. Biol.* **1998**, *19*, 210−215.

(9) Jones, A. M.; Martin, L.; Bright-Thomas, R. J.; Dodd, M. E.; McDowell, A.; Moffitt, K. L.; Elborn, J. S.; Webb, A. K. Inflammatory markers in cystic fibrosis patients with transmissible *Pseudomonas aeruginosa*. *Eur. Respir. J.* **2003**, *22*, 503−506.

(10) Bezzerri, V.; Borgatti, M.; Nicolis, E.; Lampronti, I.; Dechecchi, M. C.; Mancini, I.; Rizzotti, P.; Gambari, R.; Cabrini, G. Transcription factor oligodeoxynucleotides to NF-kappaB inhibit transcription of IL-8 in bronchial cells. *Am. J. Respir. Cell Mol. Biol.* **2008**, *39*, 86−96.

(11) Sadikot, R. T.; Zeng, H.; Joo, M.; Everhart, M. B.; Sherrill, T. P.; Li, B.; Cheng, D. S.; Yull, F. E.; Christman, J. W.; Blackwell, T. S. Targeted immunomodulation of the NF-kappaB pathway in airway epithelium impacts host defense against *Pseudomonas aeruginosa*. *J. Immunol.* **2006**, *176*, 4923−4930.

(12) Bezzerri, V.; Borgatti, M.; Finotti, A.; Tamanini, A.; Gambari, R.; Cabrini, G. Mapping the transcriptional machinery of the IL-8 gene in human bronchial epithelial cells. *J. Immunol.* **2011**, *187*, 6069−6081.

(13) Tamanini, A.; Borgatti, M.; Finotti, A.; Piccagli, L.; Bezzerri, V.; Favia, M.; Guerra, L.; Lampronti, I.; Bianchi, N.; Dall'Acqua, F.; Vedaldi, D.; Salvador, A.; Fabbri, E.; Mancini, I.; Nicolis, E.; Casavola, V.; Cabrini, G.; Gambari, R. Trimethylangelicin reduces IL-8 transcription and potentiates CFTR function. *Am. J. Physiol.: Lung Cell. Mol. Physiol.* **2011**, *300*, L380−L390.

(14) Nicolis, E.; Lampronti, I.; Dechecchi, M. C.; Borgatti, M.; Tamanini, A.; Bianchi, N.; Bezzerri, V.; Mancini, I.; Giri, M. G.; Rizzotti, P.; Gambari, R.; Cabrini, G. Pyrogallol, an active compound from the medicinal plant *Emblica officinalis*, regulates expression of pro-inflammatory genes in bronchial epithelial cells. *Int. Immunopharmacol.* **2008**, *8*, 1672−1680.

(15) Piccagli, L.; Fabbri, E.; Borgatti, M.; Bezzerri, V.; Mancini, I.; Nicolis, E.; Dechecchi, M. C.; Lampronti, I.; Cabrini, G.; Gambari, R. Docking of molecules identified in bioactive medicinal plants extracts into the p50 NF-kappaB transcription factor: correlation with inhibition of NF-kappaB/DNA interactions and inhibitory effects on IL-8 gene expression. *BMC Struct. Biol.* **2008**, *8*, 38.

(16) Nicolis, E.; Lampronti, I.; Dechecchi, M. C.; Borgatti, M.; Tamanini, A.; Bezzerri, V.; Bianchi, N.; Mazzon, M.; Mancini, I.; Giri, M. G.; Rizzotti, P.; Gambari, R.; Cabrini, G. Modulation of expression of IL-8 gene in bronchial epithelial cells by 5-methoxypsoralen. *Int. Immunopharmacol.* **2009**, *9*, 1411−1422.

(17) Piccagli, L.; Fabbri, E.; Borgatti, M.; Bianchi, N.; Bezzerri, V.; Mancini, I.; Nicolis, E.; Dechecchi, C. M.; Lampronti, I.; Cabrini, G.; Gambari, R. Virtual screening against p50 NF-kappaB transcription factor for the identification of inhibitors of the NF-kappaB-DNA interaction and expression of NF-kappaB upregulated genes. *ChemMedChem* **2009**, *4*, 2024−2033.

(18) Piccagli, L.; Borgatti, M.; Nicolis, E.; Bianchi, N.; Mancini, I.; Lampronti, I.; Vevaldi, D.; Dall'Acqua, F.; Cabrini, G.; Gambari, R. Virtual screening against nuclear factor kappaB (NF-kappaB) of a focus library: identification of bioactive furocoumarin derivatives inhibiting NF-kappaB dependent biological functions involved in cystic fibrosis. *Bioorg. Med. Chem.* **2010**, *18*, 8341−8349.

(19) Borgatti, M.; Chilin, A.; Piccagli, L.; Lampronti, I.; Bianchi, N.; Mancini, I.; Marzaro, G.; dall'Acqua, F.; Guiotto, A.; Gambari, R. Development of a novel furocoumarin derivative inhibiting NF-kappaB dependent biological functions: design, synthesis and biological effects. *Eur. J. Med. Chem.* **2011**, *46*, 4870−4877.

(20) Ghosh, G.; van Duyne, G.; Ghosh, S.; Sigler, P. B. Structure of NF-kappa B p50 homodimer bound to a kappa B site. *Nature* **1995**, *373*, 303−310.

(21) Iwai, H.; Zuger, S. Protein ligation: applications in NMR studies of proteins. *Biotechnol. Genet. Eng. Rev.* **2007**, *24*, 129−145.

(22) Hetenyi, C.; van der Spoel, D. Efficient docking of peptides to proteins without prior knowledge of the binding site. *Protein Sci.* **2002**, *11*, 1729−1737.

(23) Hetenyi, C.; van der Spoel, D. Blind docking of drug-sized compounds to proteins with up to a thousand residues. *FEBS Lett.* **2006**, *580*, 1447−1450.

(24) Verma, J.; Khedkar, V. M.; Coutinho, E. C. 3D-QSAR in drug design—a review. *Curr. Top. Med. Chem.* **2010**, *10*, 95−115.

(25) Talele, T. T.; Kulkarni, V. M. Three-dimensional quantitative structure−activity relationship (QSAR) and receptor mapping of cytochrome P-450(14 alpha DM) inhibiting azole antifungal agents. *J. Chem. Inf. Comput. Sci.* **1999**, *39*, 204−210.

(26) Walter, D. E.; Muhammad, T. D. Genetically Evolved Receptor Models (GERM): A Procedure for Construction of Atomic-Level Receptor Site Models in the Absence of a Receptor Crystal Structure. In *Genetic Algorithms in Molecular Modeling*; Devillers, J., Ed.; Academic Press: London, 1996; pp 193−210.

(27) Veselovskaya, M. V.; Shilin, S. V.; Garazd, M. M.; Khilya, V. P. Modified coumarins. 9. Synthesis of amino-acid derivatives of 3-(2,3,5-trimethyl-7-oxofuro[3,2-*g*]chromen-6-yl)propanoic acid. *Chem. Nat. Compd.* **2003**, *39*, 177−181.

(28) Nagorichna, I. V.; Dubovik, I. P.; Garazd, M. M.; Khilya, V. P. Modified coumarins. 10. Synthesis of substituted 2-(7-oxofuro[3,2-*g*]chromen-6-yl)acetic acids. *Chem. Nat. Compd.* **2003**, *39*, 253−261.

(29) Sharma, R. K.; Chopra, S.; Sharma, S. D.; Pande, V.; Ramos, M. J.; Meguro, K.; Inoue, J.; Otsuka, M. Biological evaluation, chelation, and molecular modeling studies of novel metal-chelating inhibitors of NF-kappaB-DNA binding: structure activity relationships. *J. Med. Chem.* **2006**, *49*, 3595−3601.

(30) Hearst, J. E. Psoralen photochemistry and nucleic acid structure. *J. Invest. Dermatol.* **1981**, *77*, 39−44.
(31) Nurminen, E. M.; Pihlavisto, M.; Lazar, L.; Szakonyi, Z.; Pentikainen, U.; Fulop, F.; Pentikainen, O. T. Synthesis, in vitro activity, and three-dimensional quantitative structure−activity relationship of novel hydrazine inhibitors of human vascular adhesion protein-1. *J. Med. Chem.* **2010**, *53*, 6301−6315.
(32) *Discovery Studio Modeling Environment*, release 3.1; Accelrys Software Inc.: San Diego, CA, 2005−2011.
(33) Tosco, P.; Balle, T. Open3DQSAR: a new open-source software aimed at high-throughput chemometric analysis of molecular interaction fields. *J. Mol. Model.* **2011**, *17*, 201−208.
(34) Lipkowitz, K. B.; Boyd, D. B. *Reviews in Computational Chemistry*; John Wiley & Sons, Hoboken, NJ, 1997.
(35) Gramatica, P. Principles of QSAR models validation: internal and external. *QSAR Comb. Sci.* **2007**, *26*, 794−801.
(36) Borgatti, M.; Mancini, I.; Bianchi, N.; Guerrini, A.; Lampronti, I.; Rossi, D.; Sacchetti, G.; Gambari, R. Bergamot (*Citrus bergamia* Risso) fruit extracts and identified components alter expression of interleukin 8 gene in cystic fibrosis bronchial epithelial cell lines. *BMC Biochem.* **2011**, *12*, 15.
(37) Boyce, B. F.; Yao, Z.; Xing, L. Functions of nuclear factor kappaB in bone. *Ann. N.Y. Acad. Sci.* **2010**, *1192*, 367−375.
(38) Piva, R.; Penolazzi, L.; Borgatti, M.; Lampronti, I.; Lambertini, E.; Torreggiani, E.; Gambari, R. Apoptosis of human primary osteoclasts treated with molecules targeting nuclear factor-kappaB. *Ann. N.Y. Acad. Sci.* **2009**, *1171*, 448−456.
(39) Atkinson, G. P.; Nozell, S. E.; Benveniste, E. T. NF-kappaB and STAT3 signaling in glioma: targets for future therapies. *Expert Rev. Neurother.* **2010**, *10*, 575−586.
(40) Wong, K. K.; Jacks, T.; Dranoff, G. NF-kappaB fans the flames of lung carcinogenesis. *Cancer Prev. Res.* **2010**, *3*, 403−405.
(41) Saadane, A.; Masters, S.; DiDonato, J.; Li, J.; Berger, M. Parthenolide inhibits IkappaB kinase, NF-kappaB activation, and inflammatory response in cystic fibrosis cells and mice. *Am. J. Respir. Cell Mol. Biol.* **2007**, *36*, 728−736.
(42) Cigana, C.; Nicolis, E.; Pasetto, M.; Assael, B. M.; Melotti, P. Anti-inflammatory effects of azithromycin in cystic fibrosis airway epithelial cells. *Biochem. Biophys. Res. Commun.* **2006**, *350*, 977−982.
(43) Garazd, M. M.; Garazd, Ia, L.; Ogorodniichuk, A. S.; Khilia, V. P. Synthesis of modified psoralen analogues. *Bioorg. Khim.* **2004**, *30*, 324−333.
(44) Pettersen, E. F.; Goddard, T. D.; Huang, C. C.; Couch, G. S.; Greenblatt, D. M.; Meng, E. C.; Ferrin, T. E. UCSF Chimera—a visualization system for exploratory research and analysis. *J. Comput. Chem.* **2004**, *25*, 1605−1612.
(45) *Marvin*, version 5.5.0.1, Program B; ChemAxon: Budapest, Hungary; www.chemaxon.com/products.
(46) O'Boyle, N. M.; Banck, M.; James, C. A.; Morley, C.; Vandermeersch, T.; Hutchison, G. R. Open Babel: an open chemical toolbox. *J. Cheminf.* **2011**, *3*, 33.
(47) Morris, G. M.; Huey, R.; Lindstrom, W.; Sanner, M. F.; Belew, R. K.; Goodsell, D. S.; Olson, A. J. AutoDock4 and AutoDockTools4: automated docking with selective receptor flexibility. *J. Comput. Chem.* **2009**, *30*, 2785−2791.
(48) Granovsky, A. A. *Firefly*, version 7.1.G; http://classic.chem.msu.su/gran/firefly/index.html.
(49) Schmidt, M. W.; Baldridge, K. K.; Boatz, J. A.; Elbert, S. T.; Gordon, M. S.; Jensen, J. H.; Koseki, S.; Matsunaga, N.; Nguyen, K. A.; Su, S.; Windus, T. L.; Dupuis, M.; Montgomery, J. A. General atomic and molecular electronic structure system. *J. Comput. Chem.* **1993**, *14*, 1347−1363.
(50) Pastor, M.; Cruciani, G.; Clementi, S. Smart region definition: a new way to improve the predictive ability and interpretability of three-dimensional quantitative structure−activity relationships. *J. Med. Chem.* **1997**, *40*, 1455−1464.
(51) Baroni, M.; Clementi, S.; Cruciani, G.; Costantino, G.; Riganelli, D.; Oberrauch, E. Predictive ability of regression models. Part II: Selection of the best predictive PLS model. *J. Chemom.* **1992**, *6*, 347−356.
(52) Borgatti, M.; Bezzerri, V.; Mancini, I.; Nicolis, E.; Dechecchi, M. C.; Lampronti, I.; Rizzotti, P.; Cabrini, G.; Gambari, R. Induction of IL-6 gene expression in a CF bronchial epithelial cell line by *Pseudomonas aeruginosa* is dependent on transcription factors belonging to the Sp1 superfamily. *Biochem. Biophys. Res. Commun.* **2007**, *357*, 977−983.
(53) Gambari, R.; Feriotto, G.; Rutigliano, C.; Bianchi, N.; Mischiati, C. Biospecific interaction analysis (BIA) of low-molecular weight DNA-binding drugs. *J. Pharmacol. Exp. Ther.* **2000**, *294*, 370−377.
(54) Feriotto, G.; Corradini, R.; Sforza, S.; Bianchi, N.; Mischiati, C.; Marchelli, R.; Gambari, R. Peptide nucleic acids and biosensor technology for real-time detection of the cystic fibrosis W1282X mutation by surface plasmon resonance. *Lab. Invest.* **2001**, *81*, 1415−1427.
(55) Dechecchi, M. C.; Nicolis, E.; Bezzerri, V.; Vella, A.; Colombatti, M.; Assael, B. M.; Mettey, Y.; Borgatti, M.; Mancini, I.; Gambari, R.; Becq, F.; Cabrini, G. MPB-07 reduces the inflammatory response to *Pseudomonas aeruginosa* in cystic fibrosis bronchial cells. *Am. J. Respir. Cell Mol. Biol.* **2007**, *36*, 615−624.
(56) Borgatti, M.; Mazzitelli, S.; Breveglieri, G.; Gambari, R.; Nastruzzi, C. Induction by TNF-alpha of IL-6 and IL-8 in cystic fibrosis bronchial IB3-1 epithelial cells encapsulated in alginate microbeads. *J. Biomed. Biotechnol.* **2010**, 2010.